Journal of Al-Turath University College (JATUC)
Open Access Journal
ISSN: 2074-5621
DOI: https://doi.org/10.63964/JATUC.43.2.2026.41
https://jatuc.uoturath.edu.iq/

Synthesis and Characterization of Al_2O_3 doped TiO_2 Thin Films Prepared by Pulsed Laser Deposition Technique

Zainab Saad Mahdi[1], Khalil Taha Jadaan[2*], Ali A. Sallal[3], N.A. Hassan[4], Ali Abbas Sadiq [5]

[1,2,3,4,5]Department of Physics, College of Science, University of Diyala, Diyala, Iraq.

*Correspondence email: KhalilTahaJadaan@uodiyala.edu.iq

KEYWORDS

Aluminum oxide; TiO_2 Films; Pulsed Laser Deposition; Structural optical properties.

ABSTRACT

In this study, nanostructured titanium dioxide (TiO_2) thin films were synthesized on glass substrates using the Pulsed Laser Deposition (PLD) technique (utilizing a Nd: YAG laser). The impact of aluminum oxide (Al_2O_3) doping at various concentrations (0, 1, 3, 5 wt%) on the structural and optical properties was systematically investigated. X-ray Diffraction (XRD) analysis confirmed the formation of a polycrystalline tetragonal structure for all samples. It was observed that the average crystallite size decreased with higher doping levels, correlating with an increase in the Full Width at Half Maximum (FWHM) and lattice strain. Optical characterization revealed that the optical transmittance decreases as the Al_2O_3 content increases. The pure TiO_2 film exhibited the lowest absorbance in the UV region, whereas doped films showed enhanced absorption in the visible (VIS) spectrum. Notably, the optical energy gap (E g) significantly narrowed from 3.78 eV for the pure film to 2.98 eV at 5% doping, attributed to the introduction of new localized states within the band gap. Furthermore, an increase in the refractive index and both the real and imaginary parts of the dielectric constants was observed in tandem with the doping ratio in the visible range.

1. INTRODUCTION

Titanium dioxide constitutes a semiconductor with a substantial band gap, with excellent stability as well as a diverse array of industrial applications [1]. TiO_2 thin films, characterized by their elevated refractive index, possess numerous applications within the realms of waveguides and optical coatings [2]. The three crystalline forms of titanium dioxide are as follows: brookite, which is orthogonal; rutile, which is tetragonal; and anatase, which is also tetragonal [3]. Titanium dioxide (TiO_2) has garnered significant interest recently owing to its substantial prospective purposes in the field of optical components, microelectronic devices, anti-static coatings, and photovoltaic solar cells. Capacitors or gate cells are all examples of such materials, and include electrical insulation, reflective, a variety of coatings, photonic crystals, optical waveguides and metal-based devices [4]. Numerous deposition techniques are utilized to produce thin films made of titanium dioxide, including the evaporation of electron streams [5]. Assisted deposition using an ion beam [6], direct current magnetoreactive reactivity sputtering [7], radio frequency sputtering with a reactive magnetron beam [8], a dip-coating using the sol-gel technique [9], the sol-gel spin-coating technique [10], the process of chemical vapor deposition [11], and enhanced chemical vapor deposition made possible by plasma [12]. PLD, which stands for pulsed laser deposition, is a technique that has gained popularity [13]. The PLD method is widely used to grow oxide films because it can keep the stoichiometry of the material that was made. People have used alumina (Al_2O_3) for many different things, such as electronic packaging, catalysts, and sensors [13, 14]. There are fifteen different crystallographic phases. The γ and α forms are used in a wide range of applications because they have unique properties [15]. The high surface area of γ-Al_2O_3 makes it useful for catalysis [16]. Polycrystalline α-Al_2O_3, on the other hand, is commonly used in ceramics. [17]. This study examines the impact of varying impurity ratios on the optical and structural characteristics of TiO_2 [18]. There are many studies that identify Al_2O_3:TiO_2. In 2024, Nosidlak et al. conducted a study on thin films of ZnO/TiO_2 and ZrO/Al_2O_3 atomic layer deposition. Due to the investigations conducted with

EDX, it was possible to estimate the composition of the alloys. For the purpose of determining the theoretical dependencies of the dispersion refractive indices of the alloys that were investigated, the Bruggeman effective medium approximation (EMA) model was utilized. A confirmation of the optical modeling of the ellipsometry results was provided by the EDX assessment. For the most part, the values of the refractive index that were determined by the Bruggeman EMA model are in agreement with the ellipsometry measurements [19]. In 2025, Leoard et al. identified the ratio of Al_2O_3 to TiO_2 (Leoard et al. in 2025) and conducted a study on thin films of Al_2O_3/DLC prepared using laparoscopic coatings. The CellTiterGlo assays were used to investigate the biocompatibility of these films. The results showed that the films exhibited levels of cell viability that were statistically comparable to those of the control media. It is possible that in vivo hemocompatibility is present because blood platelets that come into contact with the DLC coatings do not release any adenosine triphosphate upon contact. These films, which are distinguished by their high level of transparency, biocompatibility, and biostability, have the potential to be useful for biomedical applications that require transparent coatings. [20]. There are many studies that identify (Al_2O_3:TiO_2) (Z. Liu et al.) In 2025, they conducted a study on thin films of (TiO_2/ZnO) prepared using laser synthesis. X-ray diffraction (XRD) and transmission electron microscopy (TEM) analyses demonstrated that the composites possessed exceptional crystallinity and a core-shell structure that was clearly defined. The core layer consisted of ultrasmall TiO_2 nanoparticles, while the shell layer was composed of ZnO. Regardless of the annealing temperature, optical measurements revealed a significant amount of ultraviolet absorption, with extremely little variation in the optical band gap, which ranged from 3.30 to 3.32 eV. The annealing process had a significant impact on the photocatalytic activity, which was evaluated by observing the degradation of Rhodamine B (RhB) dye when it was exposed to ultraviolet (UV) irradiation. The samples that were annealed at a temperature of 400 degrees Celsius achieved the highest degradation efficiency of 73.3%. These findings demonstrate that the photocatalytic performance of ZnO-TiO_2 core-shell nanocomposites can be optimized through careful control of post-annealing conditions, highlighting the potential of these nanocomposites in UV-driven environmental remediation applications. [21] There are many studies that identify Al_2O_3: TiO_2 (Fahem et al.) In 2025, a study was conducted on thin films of TiO_2/SiO_2 prepared using the sol-gel method. Within the scope of this investigation, we utilized the ratios of SiO_2 to TiO_2 as follows: 1:1.1, 1:1.2, 1:1.3, and 1:1.4. The X-ray diffraction, infrared spectrum, scanning electron microscope (SEM), and atomic force microscope (AFM) were the instruments that were utilized in the examinations that were carried out. When compared to other doping ratios, the results demonstrated a significant improvement in the performance of the solar cell at particular doping ratios. This improvement was intended to be applied to the solar cell system. The findings indicate that the incorporation of SiO_2 into TiO_2 results in the formation of an amorphous phase, changes the surface morphology, and has an effect on the optical properties. As a result, the composite material is suitable for use in photocatalysis and environmental remediation applications. Not only that, but the performance of these films in solar cell applications was evaluated, and the findings revealed a significant improvement in the efficiency of power conversion. This work paves the way for their utilization in an effort to have a new horizon to improve the performance of solar cells. [22]. In 2025, Wannapop et al. conducted a study on thin films of (Sr_2TiO_4–TiO_2) prepared using dye-sensitized, heterojunction photoanodes that were manufactured during the fabrication process and incorporated into dye-sensitized solar cell (DSSC) devices, and their photovoltaic performance was evaluated while the devices were exposed to simulated sunlight. The $Sr_2TiO_4TiO_2$ heterojunction photoanode that was manufactured at a pH of 7 and subjected to reflux synthesis at 90 degrees Celsius exhibited the highest energy conversion efficiency among the samples that were tested, according to the findings that we obtained. [23]. The current study aims to prepare doped (TiO_2) thin films with different percentages of (Al_2O_3) (0, 3, and 5 wt%) using the Pulsed Laser Deposition technique to obtain films with good specifications and high homogeneity and to study the effect of (Al_2O_3) doping on the structural and optical properties of the prepared film.

2. EXPERIMENTAL

Before the deposition process, the substrates (e.g., glass, quartz, or silicon) were meticulously cleaned to ensure high-quality film adhesion. The cleaning procedure involved sequential ultrasonic cleaning in acetone, ethanol, and deionized water for 15 minutes each. Finally, the substrates were dried using a high-purity nitrogen stream before being loaded into the PLD vacuum chamber. Thin films of titanium dioxide (TiO_2) are a naturally occurring oxide primarily extracted from ilmenite, rutile, and anatase minerals found in beach sands. It is produced industrially and is characterized by its brilliant whiteness, high opacity (hiding power), and UV resistance. In industrial and food applications, its purity reaches exceptionally high levels, exceeding 99%. Aluminum oxide (Al_2O_3), commonly known as alumina, is primarily extracted from bauxite ore through the Bayer process. Its purity typically ranges from 99% to over 99.5% (tabular alumina), making it ideal for the production of ceramics and refractory materials, which were produced through the utilization of the pulsed laser deposition (PLD) technique and were characterized with varying concentrations of alumina oxide (Al_2O_3) at 0, 1, 3, and 5 wt%. Inside is where the experiment involving a vacuum chamber is carried out. The process of pulsed laser deposition is carried out, typically at a vacuum level of 10^{-3} Torr, under low pressure of a background gas for particular instances involving oxides and nitrides. An image illustrates the configuration pertaining to the laser deposition process. The directed Nd:YAG SHG Q-switched laser beam that has entered through a window causes damage to the surface of the target, which is positioned at an angle of 45 degrees. It is the substrate that is located. The surface of the target should be aligned parallel to the surface of the objective before the target. The prepared targets exhibited a uniform disk-like shape with a diameter of 25 mm. The undoped target appeared pure white, while a slight color shift was observed as the alumina doping concentration increased. All targets showed high mechanical integrity with no visible surface cracks, ensuring stability during the ablation/sputtering process. One ensures that there is a sufficient distance between the target and the substrate in order to prevent the substrate holder from obstructing the laser beam that is incident on the target. Numerous researchers periodically modify the deposition technique to achieve superior-quality films through this process. These encompass target rotation, substrate heating, and substrate positioning relative to the target. The phase composition and crystalline An X-ray diffractometer is utilized in order to conduct an analysis of the samples' structures. Model XRD 6000, manufactured by Shimadzu in Japan, utilized high-intensity Cu K radiation (1.540 mm), with a scan range of 20 to 60 degrees and a scan speed of 6 degrees per minute for the measurement. Crystalline substances and phases can be identified by comparing the X-ray diffraction patterns of samples to standard data from the JCPDS. The authors appreciate the reviewer's insightful comment. The thin films were synthesized using the Pulsed Laser Deposition (PLD) technique, chosen for its superior ability to transfer the stoichiometry of the bulk target to the substrate. In response to your suggestion, we have further elaborated on the deposition parameters, specifically the laser fluence, repetition rate, and target-to-substrate distance, to provide a clearer understanding of the film growth dynamics and crystalline quality. These revisions have been incorporated into the Experimental Section. Numerous optical techniques exist to measure film thickness, relying on the interference of light in thin films. Measurements of film thickness have been acquired using the optical interferometer technique that will be used. The interference of light beam reflections from the thin film interface and the substrate base is the foundation of this method. The He-Ne laser (0.632 μm) is employed, and the measurement of thickness is calculated using the subsequent formula [24].

$$d = \frac{\Delta x}{x} \times \frac{\lambda}{2} \tag{1}$$

Here, the variable x represents the width of the fringe, and the symbol Δx represents the symbol λ represents the wavelength of the laser, and the distance between two fringes is the quantity that is being measured as illumination. The film thickness derived from the application of equation (1) is 200 nm. The interference pattern arises from the phase difference between rays reflected from the rear surface and those reflected from the front surface.

3. RESULTS AND DISCUSSION

3.1. Structural Properties

X-ray diffraction (XRD) analysis was conducted for the prepared nanomaterials to investigate their crystal structure and crystallite size using a Shimadzu-6000 X-ray diffractometer, with a wavelength of λ = 1.54060 and a voltage of 40 kV. A display of the experimental XRD patterns of the nanomaterials that were prepared is shown in Figure 1. The characteristic peaks are obtained at angles (25.33, 25.35, 25.36, and 25.33) for pure and doped. Corresponding to the (101) crystalline planes revealed the formation of a tetragonal rutile structure of titanium dioxide (TiO_2), with lattice constants (a = b ≠ c) and angles (α = β = γ = 90). The XRD results demonstrated the pure crystalline structure of the synthesized titanium nanoparticles [25], as no other peaks were detected in the experimental XRD pattern upon doping with aluminum oxide (Al_2O_3) [26]. The appearance of new peaks was observed with increasing doping concentrations, reaching a maximum at a doping ratio of 5%, as shown in Table 1. This can be explained by the lack of incorporation of aluminum ions into the TiO_2 crystal lattice. The resulting diffraction patterns revealed that the peak width increased after doping with aluminum oxide ions, indicating that the presence of aluminum ions contributed to an increase in the crystalline growth of TiO_2. Conversely, the obtained results showed a significant decrease in crystallite size as the doping ratio increased [27].

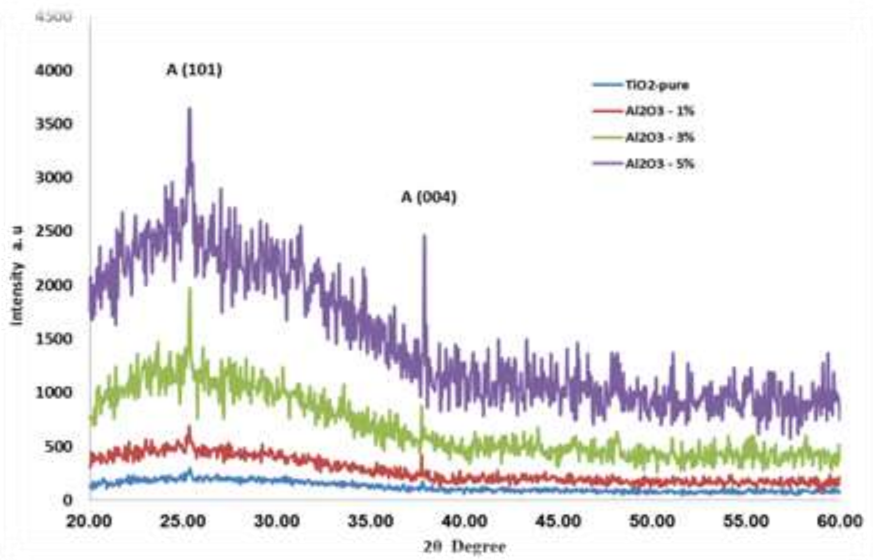

Fig. 1. XRD of TiO_2 thin films with different Al2O3 ratios (0,1,3, and 5wt%).

Table 1. The results of the structural parameters that were obtained from XRD are presented

state	2θ (Deg.)	FWHM (Deg.)	Crystalline size (nm)	d_{hkl} Exp.(Å)	d_{hkl} Std.	hkl	in Card No.
Pure TiO_2	25.33	0.30	0.028	3.517	3.512	101	1272-21
TiO_2-Al 1%	25.35	0.34	0.025	3.510	3.510	101	1272-21
TiO_2-Al 3%	25.36	0.37	0.023	3.668	3.507	101	1272-21
TiO_2-Al 5%	25.33	0.43	0. 18	3.517	3.513	101	1272-21

3.2. Optical Properties

For practical uses, it is important to have a good understanding of the optical properties of optical semiconductor materials, which are closely related to the material's crystal structure and energy level configuration. The transmission of films is usually affected by the film's thickness, surface properties, type of material, crystal structure, substrate temperature, and the sum of the films' absorbance and reflectance. As the percentage of impurities rises, the transmission goes down, as shown in Fig. 2. In thin films made of titanium dioxide with varying impurity ratios, the transmittance spectrum varies as a function of wavelength [28].

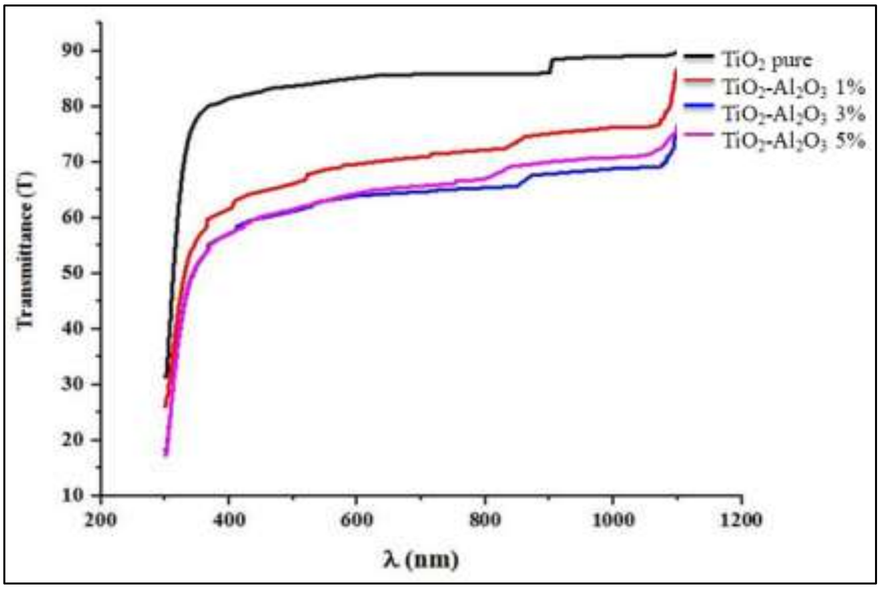

Fig. 2. The transmittance spectrum varies as a function of wavelength for TiO_2 thin films with different Al_2O_3 ratios (0,1,3, and 5wt%).

It can be observed from Figure 3 that the absorptivity is inversely proportional to the wavelength, as the absorptivity decreases with increasing wavelength, reaching its lowest value at a wavelength of 1100 nm for each and every film that has been prepared.

This indicates that the energy of the photon that is incident on the semiconductor is lower than the energy of the bandgap of the semiconductor. As a result, the electron does not become excited and does not transition fro m the valence band to the conduction band. This is why the absorptivity decreases with increasing wavelength. [29]. Doping pure (TiO_2)with varying percentages of (Al_2O_3) causes the chipping rate to increase due to absorption, which in turn decreases the processed film value. An absorbance measurement range of up to 22% is possible for (Al_2O_3). This is the result of atoms of impurities being introduced into the crystalline structure of the film while it is being prepared. To improve absorption, energy levels can be generated between the energy bands, as shown in (Fig. 3).

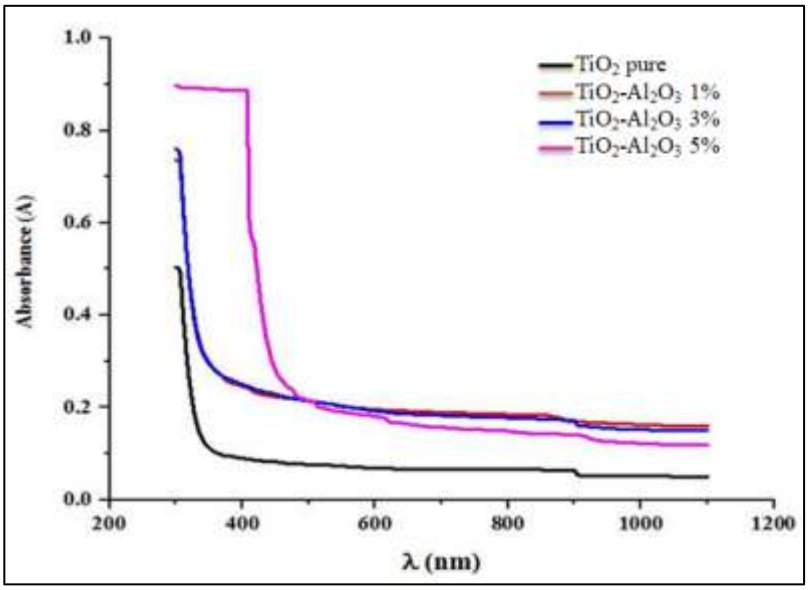

Fig. 3. The relationship between the wavelength and the variation of the absorption spectrum for TiO_2 thin films with different Al_2O_3 ratios (0,1,3, and 5 wt%).

Illustrates the relationship between the energy band gap and photon energy for the synthesized samples. It is observed that the optical band gap (Eg) exhibits a progressive decrease as the doping concentration increases from 0 to 5 wt.% [30], as shown in Fig. 4. This reduction in the band gap can be attributed to the creation of localized donor/acceptor levels within the forbidden gap, which facilitates electronic transitions and subsequently shifts the absorption edge toward longer wavelengths [31]. X-ray diffraction (XRD) measurements showed a good agreement between the two studies. However, optical measurements revealed consistency in the refractive index and the real dielectric constant, while discrepancies were observed in the energy gap and the imaginary dielectric constant [32]. X-ray diffraction (XRD) measurements showed a lack of agreement between the two studies. Similarly, the optical measurements demonstrated no consistency (or discrepancies) as well [33], as shown in Table 2.

Table 2. Energy gap values for TiO_2 thin films with different Al_2O_3 ratios (0,1,3, and 5wt%).

Energy gap (eV)	Value
0%	3.78
1%	3.38
3%	3.25
5%	2.98

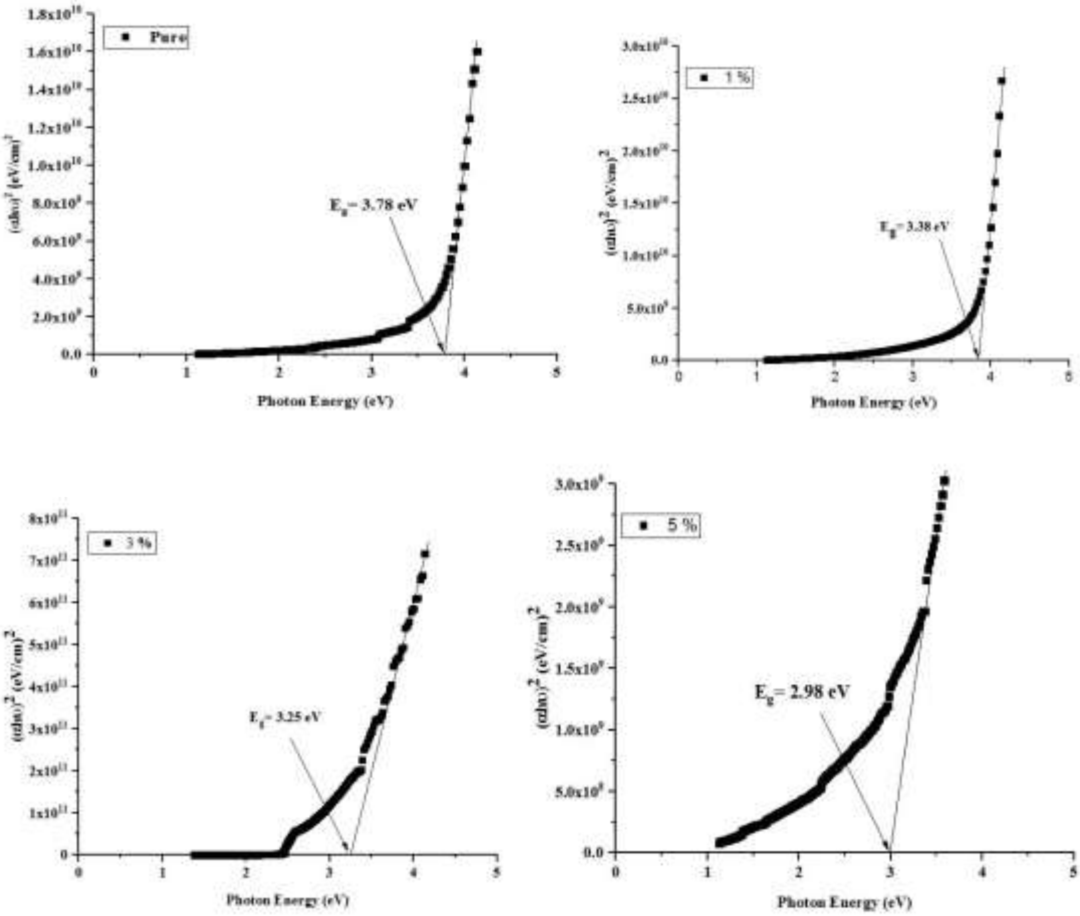

Fig. 4. The plots of (αhv)2 versus photon energy (hv) of TiO_2 thin films with different Al_2O_3 ratios (0,1,3, and 5 wt%). titanium dioxide (TiO_2) with different Al_2O_3 ratios

Figure 5 illustrates the relationship between the wavelength and the refractive index values of the films that have been prepared. Through the use of the figure, it is possible to see that the refractive index values for all pure and doped films are the same decrease as the wavelength increases. This behavior is attributed to the fact that the doping process was unable to displace the impurity atoms from the pure material. Furthermore, there is a correlation between the decrease in the refractive index and a weakening of the reflected radiation.

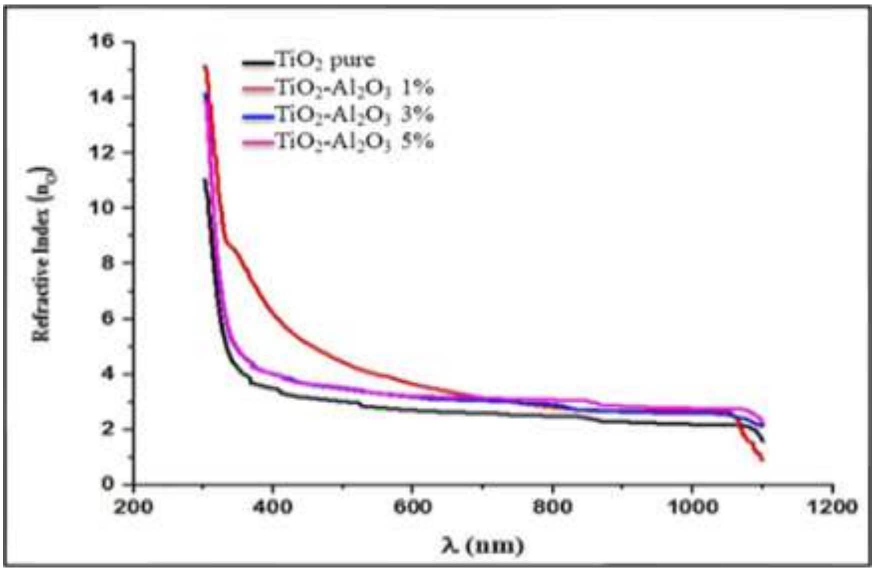

Fig.5. Variation of the refractive index with wavelength spectrum for TiO_2 thin films with different Al_2O_3 ratios (0,1,3, and 5 wt%).

Figures 6 and 7 illustrate the relationship between both the real and imaginary dielectric constants, as well as the wavelength, for the films that have been prepared and can be calculated by using the following equation [34]. Figure 6 demonstrates that the value of the real dielectric constant is an important factor to consider, which decreases for both pure and doped materials. This decrease is attributed to the lack of energy generation from induced dipoles as a result of the doping increase. Regarding (Fig. 7), it shows that there is a decrease in the imaginary dielectric constant with increasing wavelength for both pure and doped films. This behavior occurs because the doping process does not increase the polarization ratio, thereby preventing significant energy absorption and the formation of new energy levels [35].

$$(n - ik_{ex})^2 = \varepsilon_r - i\varepsilon_i \quad (2)$$

$$\varepsilon_r = n^2 - k_{ex}^{\ 2} \quad (3)$$

$$\varepsilon_i = 2nk_{ex.} \quad (4)$$

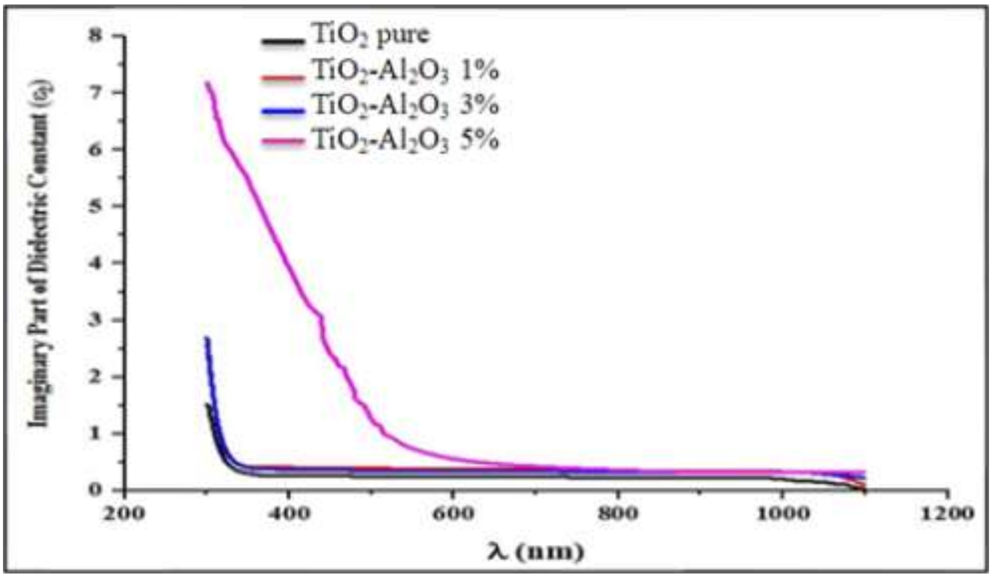

Fig. 6. The relationship between the real dielectric constant and wavelength for TiO_2 thin films with different Al_2O_3 ratios (0,1,3, and 5 wt%).

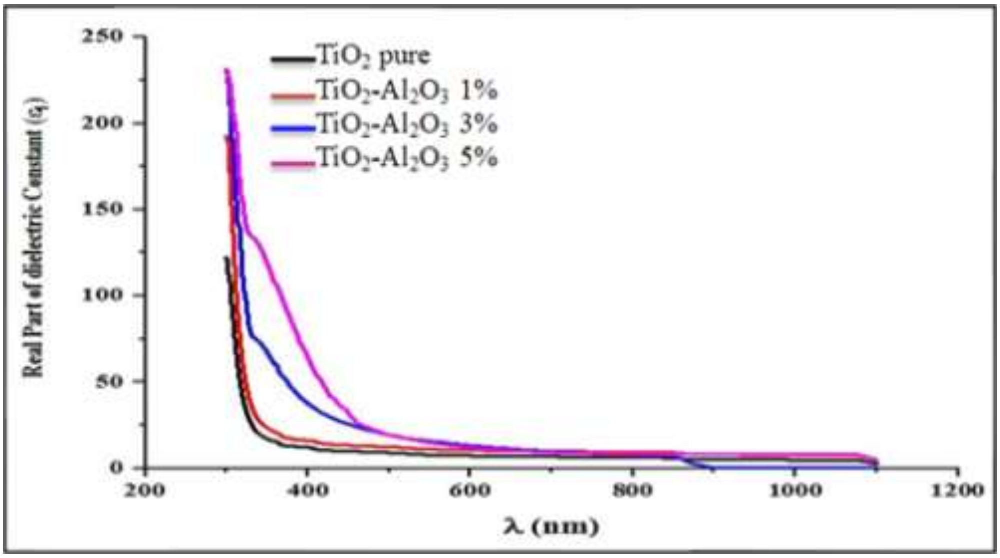

Fig. 7. The imaginary dielectric constant for TiO_2 thin films with different Al_2O_3 ratios (0,1,3, and 5 wt%).

4. CONCLUSIONS

Examination using X-ray diffraction reveals the films are composed of polycrystalline material with a favorable orientation along the a-axis (101) direction, exhibiting a cubic phase structure of TiO_2:Al_2O_3 for both pure and doped samples. The phase is rutile. The optical transmission of the films decreases as the doping ratio increases from 0 to 3% and then increases; the absorption edge demonstrates a red shift, and the optical. Band gap energy decreases from 3.78 eV to 2.98 eV as the concentration of Al_2O_3 escalates from 0 to 5%. The values of the optical absorption coefficient and the extinction coefficient increase with higher doping concentrations. The refractive index is observed to rise with the augmentation of impurities within the visible spectrum. The results indicate that both the real (εr) and imaginary components of the dielectric constant increase with the wavelength for TiO_2 thin films containing varying proportions of impurities.

Conflict of interest

The authors declare that the research was conducted in the absence of any commercial or financial " relationships that could be construed as a potential conflict of interest."

Consent for Publication

Not applicable. This manuscript does not contain any individual person's data in any form (including " "individual details, images, or videos), and therefore consent for publication is not required.

Availability of Data and Materials

The data supporting the findings of this study are included within the article.

Authors' Contributions

A.B. conceived and designed the study.
A.B. and C.D. prepared the materials and performed the experiments.
and optical properties. C.D. and E.F. carried out the structural properties and analyzed the data.
G.H. contributed to data interpretation and manuscript writing.
All authors reviewed and approved the final manuscript.

Funding

There is no fund

5. REFERENCES

[1] M. Ijaz and M. Zafar, "Titanium dioxide nanostructures as efficient photocatalyst: Progress, challenges and perspective," Int. J. Energy Res. 2021, vol. 45, (no. 3), pp. 3569–3589, DOI: 10.1002/er.6079.

[2] D. Silva et al., "Sputtering deposition of TiO2 thin film coatings for fiber optic sensors," in Proc. Photonics, May 2022, vol. 9,(no. 5),(p. 342), doi.org/10.3390/photonics9050342.

[3] L. Stephen, Titanium Dioxide Versatile Solid Crystalline: An Overview. London, UK: IntechOpen, 2020, DOI: 10.5772/intechopen.92056.

[4] S. Ge, D. Sang, C. Li, Y. Shi, Q. Wang, and D. Xiao, "Research progress and future perspectives on photonic and optoelectronic devices based on p-type boron-doped diamond/n-type titanium dioxide heterojunctions: A mini review," Nanomaterials,2025, vol. 15,(no. 13), p. 1003, doi.org/10.3390/nano15131003.

[5] Y. H. Wang, K. H. Rahman, C. C. Wu, and K. C. Chen, "A review on the pathways of the improved structural characteristics and photocatalytic performance of titanium dioxide (TiO2) thin films fabricated by the magnetron-sputtering technique," Catalysts,2020, vol. 10, (no. 6), p. 598, doi.org/10.3390/catal10060598.

[6] C. Yang, H. Fan, Y. Xi, J. Chen, and Z. Li, "Effects of depositing temperatures on structure and optical properties of TiO2 film deposited by ion beam assisted electron beam evaporation," Appl. Surf. Sci.,2008, vol. 254,(no. 9), pp. 2685–2689, doi:10.1016/j.apsusc.2007.10.006.

[7] C. Tavares et al., "Reactive sputtering deposition of photocatalytic TiO2 thin films on glass substrates," Mater. Sci. Eng. B,2007, vol. 138, (no. 2), pp. 139–143, doi:10.1016/j.mseb.2005.11.043.

[8] S. C. Ray, D. K. Mishra, A. B. Panda, H. T. Wang, S. Bhattacharya, and W. F. Pong, "Temperature-dependent electronic structure of TiO2 thin film deposited by the radio frequency reactive magnetron sputtering technique: X ray absorption near-edge structure and X ray photoelectron spectroscopy," The Journal of Physical Chemistry C,2022, vol. 126, (no. 20), pp. 8947-8952, doi.org/10.1021/acs.jpcc.2c02311.

[9] M. M. Islam, A. G. Ranga, V. Borra, and D. G. Georgiev, "Copper tantalum nitride (CuTaN2) thin films prepared by reactive radio-frequency magnetron sputtering," Appl. Phys. A, 2024, vol. 130, (no. 6), p. 376, doi.org/10.1007/s00339-024-075370.

[10] S. O. Oloruntoba, Z. Zainal, Y. Sulaiman, and R. M. Zawawi, "Fabrication of Zinc Oxide thin films by Sol-Gel dip coating process," J. Nanosci. Res. Rep., 2024, vol. 6,(no. 169), pp. 2–6, DOI: doi.org/10.47363/JNSRR/2024(6)169.

[11] K. P. Devi, P. Goswami, and H. Chaturvedi, "Fabrication of nanocrystalline TiO2 thin films using Sol-Gel spin coating technology and investigation of its structural, morphology and optical characteristics," Appl. Surf. Sci. 2022, vol. 591, p. 153226, doi.org/10.1016/j.apsusc.2022.153226.

[12] L. Sun et al., "Chemical vapour deposition," Nat. Rev. Methods Primers, 2021, vol. 1, (no. 1), p. 5, doi.org/10.1038/s43586-020-00005-y.

[13] K. Yi et al., "Plasma-enhanced chemical vapor deposition of two-dimensional materials for applications," Acc. Chem. Res.,2021, vol. 54, (no. 4), pp. 1011–1022, doi.org/10.1021/acs.accounts.0c00757.

[14] A. J. Haider, T. Alawsi, M. J. Haider, B. A. Taha, and H. A. Marhoon, "A comprehensive review on pulsed laser deposition technique to effective nanostructure production: Trends and challenges," Opt. Quantum Electron., 2022, vol. 54,(no. 8), p. 488,doi.org/10.1007/s11082-022-03786-6.

[15] R. J. D. Tilley, Crystals and Crystal Structures, 2nd ed. Hoboken, NJ, USA: John Wiley & Sons, 2020.

[16] W. Trisunaryanti, M. F. Pradipta, J. Purbonegoro, and A. E. Pratiwi, "Preparation and performance of 3-APTMS-modified NiO/\gamma-Al$_2O_3$ for high-efficiency biodiesel production from used palm oil," J. Environ. Chem. Eng.,2025, vol. 13, (no. 3), Art. no. 116149, doi.org/10.1016/j.jece.2025.116149.

[17] F. Konstantiniuk, M. Tkadletz, C. Kainz, C. Czettl, and N. Schalk, "Mechanical properties of single and polycrystalline \alpha-Al$_2O_3$ coatings grown by chemical vapor deposition," Surf. Coat. Technol., 2021, vol. 410, (Art. no. 126959), doi.org/10.1016/j.surfcoat.2021.126959.

[18] K. Prajapat, U. Mahajan, M. Dhonde, K. Sahu, and P. M. Shirage, "Synthesis and characterization of TiO2 nanoparticles: Unraveling the influence of copper doping on structural, surface morphology, and optical properties, Chem. Phys. Impact,2024, vol. 8, (Art. no.100607), doi.org/10.1016/j.chphi. 2024.100607.

[19] N. Nosidlak et al., “Thermo-optical, structural, and morphological characterization of ZnO: PQX composite thin films”, Chem. Phys. Impact, 2024, vol. 8, (Art. no. 100607),doi.org/10.24425 /bpasts.2025.157064.

[20] N. Nosidlak et al., "The optical properties of thin films alloys of ZnO, TiO2 and ZrO2 with Al2O3 synthesised by atomic layer deposition," Thin Solid Films, 2025, 15(24), 12870, doi.org/10.3390/app152412870.

[21] R. L. Leonard et al., "Biocompatibility of Al2O3-doped diamond-like carbon laparoscope coatings," Coatings, 2025, vol. 15, (no. 4), p. 437, doi.org/10.3390/coatings15040437.

[22] Z. Liu, K. Li, and R. X. Wang, "Laser synthesis and photocatalytic properties of ultrasmall TiO2 anchored ZnO core-shell nanoparticles," J. Ovonic Res., 2025, vol. 21, (no. 5), doi.org/10.15251/JOR.2025.215.591.

[23] M. Q. Fahema et al., "Preparation and characterization of SiO2-enhanced TiO2 thin films for solar cell applications," J. Ovonic Res., 2025, vol. 21, (no. 4), pp. 419–430, doi.org/10.15251/JOR.2025.214.419.

[24] S. Wannapop et al., "Fabrication of Sr2TiO4–TiO2 heterojunction photoanode dye-sensitized solar cells applications," J. Ovonic Res.,2025, vol. 21,(no. 3), pp. 377–385, doi.org/10.15251/JOR.2025.213.377.

[25] M. Lal, P. Sharma, and C. Ram, “Calcination temperature effect on titanium oxide (TiO2) nanoparticles synthesis,” Optik, 2021, vol. 241, p. 166934, Sep. doi.org/10.1016/j.ijleo.2021.166934.

[26] T. Tangcharoen, “Synthesis and characterization of 3d transition metal–doped aluminum oxide powders with enhanced photodegradation performance under sunlight irradiation,” J. Aust. Ceram. Soc., 2023, vol. 59,(no. 1), pp. 29–42.

[27] S. Vadivel and G. Rajarajan, "Effect of Mg doping on structural, optical and photocatalytic activity of SnO2 nanostructure thin films," J. Mater. Sci. Mater. Electron.,2015, vol. 26, pp. 3155–3162.

[28] M. M. Rashad et al., "Photocatalytic decomposition of dyes using ZnO doped SnO2 nanoparticles prepared by solvothermal method," Arab. J. Chem.,2014, vol. 7, pp. 71–77. [29] A. T. Abood et al., "Structural and optical properties of nanocrystalline SnO2 thin films growth by electron beam evaporation," in AIP Conf. Proc.,2020, vol. 2213, (no. 1), p. 020036, doi.org/10.1063/5.0000454.

[30] X. Liu, S. Chen, M. Li, and X. Wang, "Synthesis and characterization of ferromagnetic cobalt-doped tin dioxide thin films," Thin Solid Films,2007, vol. 515, (no. 17), pp. 6744–6748, doi.org/10.1016/j.tsf.2007.02.004.

[31] A. Taşer, M. E. Güldüren, and H. Güney, "Fe doping effects in MgO thin films grown with SILAR technique," Mater. Chem. Phys., 2021, vol. 272, p. 124993, doi.org/10.1016/j.matchemphys.2021.124993.

[32] S. Aksay, "Effects of Al dopant on XRD, FT-IR and UV–vis properties of MgO films," Phys. B Condens. Matter,2019, vol. 570, pp. 280–284, doi.org/10.1016/j.physb.2019.06.020. [33] W. A. Al-Taa'y and B. A. Hasan, "Structural, morphological and optical properties of spray pyrolysis TiO2: GO nano films," IOP Conf. Ser. Mater. Sci. Eng., 2020,vol. 928, (no. 7), p. 072036, doi:10.1088/1757899X/928/7/072036.

[34] L. Kazmarski and A.H.Clark, "Polycrystalline and Amorphous Thin Films and Devices", Edited by Lawrence Academic Press, New York, 1980.

[35] S. Mahmood and B. A. Hasan, "Effect of dopant concentration on the structural, optical and sensing properties of (SnO2) 1-x (TiO2: CuO) x sprayed films," Baghdad Sci. J., 2019, vol. 16, (no. 2), p. 8, doi.org/10.21123/bsj.2019.16.2.0361.

Journal of Al-Turath University College (JATUC)
Open Access Journal
ISSN: 2074-5621
DOI: https://doi.org/10.63964/JATUC.43.2.2026.41
https://jatuc.uoturath.edu.iq/

تصنيع وخصائص اغشية اوكسيد التيتانيوم المطعمة باوكسيد الالومينا بتقنية الترسيب بالليزر النبضي

زينب سعد مهدي[1]، خليل طه جدعان[2]، علي عبدالستار صلال[3]، نور عبدالرزاق حسن[4]، علي عباس صادق[5]

[1،2،3،4،5] قسم الفيزياء، كلية العلوم، جامعة ديالى، ديالى، العراق.

* البريد الإلكتروني للتواصل: KhalilTahaJadaan@uodiyala.edu.iq

الخلاصة

في هذه الدراسة، تم تحضير أغشية رقيقة من ثاني أكسيد التيتانيوم (TiO_2) نانوية التركيب على ركائز زجاجية باستخدام تقنية الترسيب بالليزر النبضي (PLD) (باعتماد ليزر Nd:YAG). تم استقصاء تأثير التشويب بأكسيد الألومنيوم (Al_2O_3) بتركيزات وزنية مختلفة (0، 1، 3، 5%wt) على الخصائص التركيبية والبصرية بشكل منهجي. أكد تحليل حيود الأشعة السينية (XRD) تشكّل بنية رباعية الأضلاع (Tetragonal) متعددة التبلور لجميع العينات. ولوحظ أن متوسط الحجم البلوري تناقص مع زيادة مستويات التشويب، وهو ما ارتبط بزيادة في عرض القمة عند منتصف الارتفاع (FWHM) والانفعال الشبكي (Lattice strain). أظهرت القياسات البصرية أن النفاذية الضوئية تنخفض مع زيادة محتوى Al_2O_3. وسجل غشاء TiO_2 النقي أقل امتصاصية في المنطقة فوق البنفسجية (UV)، بينما أظهرت الأغشية المشوبة امتصاصاً محسناً في الطيف المرئي (VIS). ومن الملاحظ أن فجوة الطاقة البصرية (Eg) تضاءلت بشكل كبير من 3.78 إلكترون فولت للغشاء النقي إلى 2.98 إلكترون فولت عند تركيز تشويب 5%، ويُعزى ذلك إلى استحداث مستويات موضعية جديدة داخل فجوة الحزمة. علاوة على ذلك، لوحظت زيادة في معامل الانكسار والجزءين الحقيقي والخيالي لثوابت العزل الكهربائي بالتزامن مع زيادة نسبة التشويب في المدى المرئي.

الكلمات المفتاحية
أكسيد الألومنيوم؛ أغشية ثاني أكسيد التيتانيوم؛ الترسيب بالليزر النبضي؛ الخصائص البصرية الهيكلية.